

Migration of adhesive glioma cells: Front propagation and fingering

Evgeniy Khain,¹ Mark Katakowski,² Nicholas Charteris,¹ Feng Jiang,² and Michael Chopp^{1,2}

¹*Department of Physics, Oakland University, Rochester, Michigan 48309, USA*

²*Department of Neurology, Henry Ford Hospital, Detroit, Michigan 48202, USA*

(Received 17 August 2011; revised manuscript received 11 May 2012; published 5 July 2012)

We investigate the migration of glioma cells as a front propagation phenomenon both theoretically (by using both discrete lattice modeling and a continuum approach) and experimentally. For small effective strength of cell-cell adhesion q , the front velocity does not depend on q . When q exceeds a critical threshold, a fingeringlike front propagation is observed due to cluster formation in the invasive zone. We show that the experiments correspond to the transient regime, before the regime of front propagation is established. We performed an additional experiment on cell migration. A detailed comparison with experimental observations showed that the theory correctly predicts the maximal migration distance but underestimates the migration of the main mass of cells.

DOI: [10.1103/PhysRevE.86.011904](https://doi.org/10.1103/PhysRevE.86.011904)

PACS number(s): 87.18.Gh, 05.40.-a, 87.18.Hf, 87.10.Hk

I. INTRODUCTION

Glioblastoma multiforme is a highly invasive and malignant brain tumor [1,2]. Glioma cells not only divide (proliferate) but are also motile; a cell on a substrate is able to migrate its own diameter in 5–10 min. Thus, cells detach from the primary brain tumor and actively move away to the extracellular matrix. Therefore, even if the tumor core is taken out by a surgery, many invasive cells remain intact [3]. Here we try to investigate the collective migration of glioma cells by using both a discrete stochastic lattice approach and a continuum modeling. We also performed *in vitro* experiments to verify some of the theoretical predictions.

Collective cell migration (such as in wound healing) can be described in terms of propagating cell fronts. The standard equation that describes a front propagating from the stable state (where cells are densely packed, $u = 1$, where $u = \rho/\rho_c$) to the unstable state (where there are no cells, $u = 0$) is the Fisher-Kolmogorov (or FKPP) equation, first formulated to examine the motion of advantageous genes [4]:

$$\frac{\partial u}{\partial t} = D \frac{\partial^2 u}{\partial x^2} + \alpha u(1 - u). \quad (1)$$

Here, D is the diffusion coefficient and α is the proliferation rate. It is known that sufficiently sharp initial conditions lead to a front moving with the minimal velocity $v_{FK} = 2\sqrt{D\alpha}$. Equation (1) can be derived from the underlying microscopic lattice model, where a cell on a lattice can proliferate to an empty neighboring site or jump there with probabilities proportional to α and D , respectively (see, for example, Refs. [5,6]). This derivation assumes no correlations between the neighboring sites, so it is valid only in the limit of small $\epsilon = \alpha/(D/a^2)$, where a is a lattice spacing (a cell diameter). This is exactly what happens for glioma cells, since the typical proliferation time is on the order of a day. The Fisher-Kolmogorov equation proved to be quite powerful in the context of tumor growth: it described tumor invasion and reproduced local tumor recurrence after a surgery [7,8]. However, the FKPP equation has a serious drawback: it does not take into account the important process of cell-cell adhesion, which can lead to qualitatively different patterns of cell migration. For example, motile glioma cells can form clusters *in vitro* [9] and

in vivo [10]; these clusters may potentially develop to recurrent brain tumors. Therefore, the problem of continuum modeling of cell-cell adhesion has recently attracted much attention [11]. In this study, we investigate front propagation phenomenon in the framework of the FKPP equation with nonlinear diffusion, taking into account cell-cell adhesion (Sec. II), and analyze the structure of front interface (Sec. III). Section IV presents new experimental observations. Section V includes a brief discussion and summary of our results.

II. FRONT PROPAGATION FOR SMALL CELL-CELL ADHESION

Motile glioma cells migrating on a substrate can be described as agents moving on a two-dimensional square lattice. Each lattice site can be empty or occupied by a cell, so the size of a lattice site, a , equals the effective cell diameter (of the order of $20 \mu\text{m}$). The dynamics of the model is the following. A cell is picked at random and then one of the four nearest neighboring sites is randomly chosen. If this site is empty, then a cell can proliferate or migrate there with a certain probability. The probability for proliferation is $\bar{\alpha}(n)$ (we will discuss possible forms of this function later on), while the probability for migration is $[1 - \bar{\alpha}(n)] \times (1 - q)^n$. Here n is the number of nearest neighbors (which can vary from 0 to 4) and q is the adhesion parameter ($0 \leq q < 1$) that characterizes the strength of cell-cell adhesion. Indeed, a cell with $q > 0$ has a smaller probability to detach from its neighbors and migrate away compared to the case of zero adhesion, $q = 0$. Now, one can study front propagation on a lattice, initially putting cells into the left part of a two-dimensional system ($x < 0$), while the right part ($x > 0$) is initially empty. Then cells start migrating and proliferating into the right part of the system. Averaging over many numerical simulations of the model, one can observe how the density profile $u(x)$ changes with time. After a transient period, the relatively sharp initial cell density profile develops into the propagating front $u(\xi = x - vt)$ [12,13]. In order to analyze the dependence of the front velocity v on the adhesion parameter q , we need to derive the macroscopic continuum equation that corresponds to the microscopic lattice model presented above.

For small q , this derivation for a two-dimensional system was recently performed [14]. Consider for simplicity a one-dimensional system. Considering times much longer than the diffusion time τ (5–10 min, which is a typical time for a cell to travel a distance equal to its diameter) and lengths much larger than the lattice distance a , one can write the master equation for the probability P_n that the site number n is occupied [the same equation can be written for the density of particles on site n , since $u = 1 \times P_n + 0 \times (1 - P_n)$]:

$$\begin{aligned} \tau \dot{P}_n = & -P_n(1 - P_{n+1})[(1 - \bar{\alpha})(1 - q)^{P_{n-1}+P_{n+1}}]/2 \\ & - P_n(1 - P_{n-1})[(1 - \bar{\alpha})(1 - q)^{P_{n-1}+P_{n+1}}]/2 \\ & + P_{n-1}(1 - P_n)[(1 - \bar{\alpha})(1 - q)^{P_{n-2}+P_n}]/2 \\ & + P_{n+1}(1 - P_n)[(1 - \bar{\alpha})(1 - q)^{P_n+P_{n+2}}]/2 \\ & + P_{n-1}(1 - P_n)[\bar{\alpha}/2] + P_{n+1}(1 - P_n)[\bar{\alpha}/2]. \end{aligned} \quad (2)$$

The first four terms represent jumps from site n to sites $n - 1$ and $n + 1$, and vice versa; the last two terms describe proliferation into site n . Let us discuss the first term. For a cell to jump from site n to site $n + 1$, the site n should be occupied and the site $n + 1$ should be empty. To write this as a product $P_n(1 - P_{n+1})$, we need to neglect correlations between P_n and P_{n+1} ; this assumption is reasonable when both q and $\bar{\alpha}$ are small parameters. The product $P_n(1 - P_{n+1})$ is multiplied by the probability of a jump. Note that one can add P_{n+1} to the power of $1 - q$ since the entire term is not zero only when $P_{n+1} = 0$. The next step is expanding P_{n-1} and P_{n+1} in a Taylor series up to the second order terms. For example,

$$\begin{aligned} (1 - q)^{P_{n-1}+P_{n+1}} & \simeq (1 - q)^{2P+a^2 \partial^2 P / \partial x^2} \\ & \simeq (1 - q)^{2P} \left(1 + a^2 \ln(1 - q) \frac{\partial^2 P}{\partial x^2} \right), \end{aligned}$$

where $x = an$ will be a continuum coordinate. After some algebra, one arrives at the Fisher-Kolmogorov-like reaction-diffusion equation with a nonlinear diffusion coefficient:

$$\frac{\partial P}{\partial t} = \frac{\partial}{\partial x} \left[\bar{D}(P) \frac{\partial P}{\partial x} \right] + \frac{\bar{\alpha}}{\tau} P(1 - P) + \frac{a^2 \bar{\alpha} (1 - P)}{2\tau} \frac{\partial^2 P}{\partial x^2}, \quad (3)$$

where $\bar{D}(P) = [(a^2/\tau)(1 - \bar{\alpha})/2] \times (1 - q)^{2P} [1 + 2P(1 - P) \ln(1 - q)]$. One can safely neglect the contribution to the diffusion term [the last term in Eq. (3)] that comes from proliferation to the neighboring sites, since $\bar{\alpha} \ll 1$; in addition, one can neglect $\bar{\alpha}$ in the expression for \bar{D} . Measuring the distance in units of a and time in units of τ , one can write the equation for the normalized cell density u (now, in two dimensions) as

$$\frac{\partial u}{\partial t} = \frac{\partial}{\partial x} \left[\bar{D}(u) \frac{\partial u}{\partial x} \right] + \bar{\alpha} u (1 - u), \quad (4)$$

where $\bar{D}(u) = (1 - q)^{4u} [1 + 4u(1 - u) \ln(1 - q)]/4$ [14].

We would like to add a comment related to the speed of front propagation in continuum and discrete lattice models. Fronts in the FKPP equation cannot propagate with velocity smaller than $v_{FK} = 2\sqrt{\bar{D}\bar{\alpha}}$. On the other hand, front velocity should be much smaller than the *microscopic* velocity, defined as the ratio between the lattice distance and the diffusion time: $v_{\text{micr}} = a/(4\tau)$, where v_{micr} corresponds to a random

cell jump to one of the four neighboring sites. To make the continuum model consistent with the underlying lattice model, one needs to demand $v_{FK} \ll a/(4\tau)$; see Ref. [15] for a detailed discussion of front propagation with diffusion with a finite velocity and the FKPP local dynamics. This leads to the following strong inequality $t_{\text{prolif}} = \tau/\alpha \gg 16\tau$, so the typical proliferation time should be much larger than the typical diffusion time. Note that we used this assumption, when deriving Eq. (3) from the discrete lattice model. Also, this strong inequality is consistent with experimental observations for glioma cells.

We look for the solution of Eq. (4) in the form of a propagating front, $u(x, t) = u(\xi = x - vt)$. Similarly to the Fisher-Kolmogorov equation, linearization in the tail region (near $u = 0$) yields the minimal front velocity. Therefore, nonlinear diffusion has no effect on the minimal velocity. Knowing the velocity of front propagation, we can substitute $u(x, t) = u(\xi = x - vt)$ into Eq. (4) and solve the resulting ordinary differential equation in MATLAB. The resulting front profiles are shown in Fig. 1. Interestingly, the profiles almost do not depend on the adhesion parameter q . Consider now sharp initial conditions $u(x < 0) = 1$, $u(x > 0) = 0$. How much time does it take to develop the front, shown in Fig. 1? In particular, how does the front velocity v approach the limiting front speed v_{FK} ? In case of the standard FKPP equation, the answer to this question is known [16]. To the leading order, the velocity difference δv is inversely proportional to time,

$$\delta v \equiv v_{FK} - v = \frac{3}{2\lambda t}, \quad (5)$$

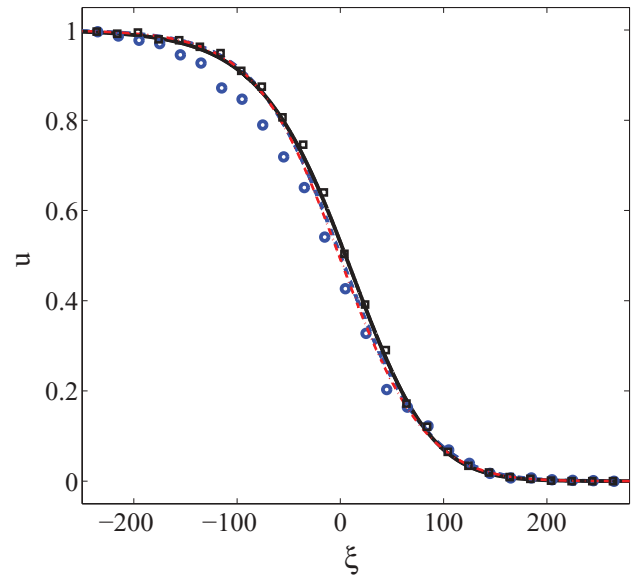


FIG. 1. (Color online) Cell density profiles for $q = 0.1$ (solid line) and $q = 0.6$ (dashed line) as obtained from analysis of Eq. (4) by looking for a solution in the form of a propagating front $u(x, t) = u(\xi = x - vt)$. The two curves are very close to each other and almost indistinguishable from the cell density profile obtained from the solution of the full time-dependent Eq. (4) at large times (dash-dotted line). Symbols denote the density profiles obtained from simulations of the discrete stochastic lattice model. Circles correspond to $q = 0.6$; squares correspond to $q = 0.1$; the results were averaged over 100 simulations in each case. $\bar{\alpha} \simeq 0.0006$.

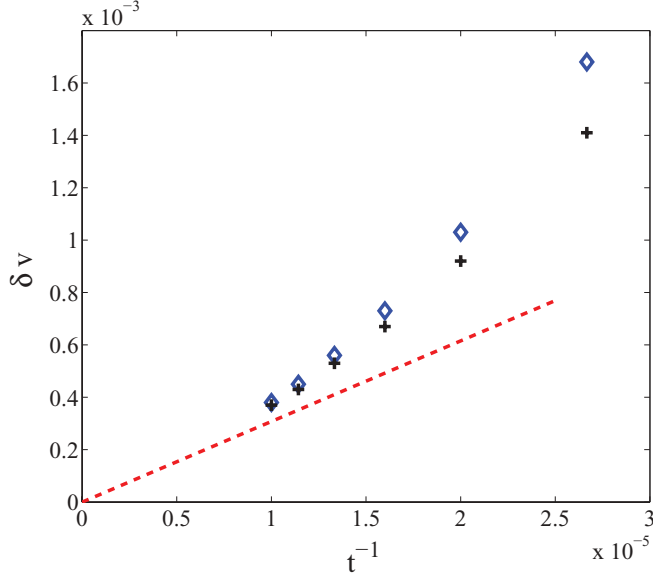


FIG. 2. (Color online) Velocity of front propagation ($\delta v = v_{FK} - v$) as a function of inverse time. For large time, the front speed v reaches the minimal front speed in the Fisher-Kolmogorov equation, v_{FK} , independently of the adhesion parameter q . The dashed curve shows the universal long-time asymptotics given by Eq. (5); symbols are computed by solving Eq. (4) numerically. The parameters are $\bar{\alpha} \simeq 0.0006$, $q = 0.1$ (pluses), and $q = 0.6$ (rhombi).

where λ is the exponent governing the decay of front profile: the tail of $u(\xi)$ decays as $\exp(-\lambda\xi)$. We checked that the same universal behavior occurs for the nonlinear diffusion; see Fig. 2. Interestingly, the large time asymptotics does not depend on the adhesion parameter q , although the subleading terms seem to depend on q : the front velocity v approaches v_{FK} faster for smaller values of q . We have also checked that the density profile at large times agrees with the one obtained from the front propagation analysis, as in Fig. 1.

To test the theoretical results, we performed long-time simulations of the underlying discrete lattice model for various adhesion parameters. The cell density profiles obtained in simulations are in a good agreement with theoretical results; see Fig. 1. We have also measured the velocity of propagating fronts, averaging over 100 runs for every time point. Our observations showed that the discrete velocity first increases with time and then saturates at large times, as expected. The values of the obtained velocities are, however, by 5–10% smaller than v_{FK} ; see Fig. 3. This discrepancy was observed earlier in the case of zero adhesion [17] due to correlations caused by nonzero proliferation. Nonzero adhesion also induces correlations between the neighboring sites. Although the theoretical front velocity does not depend on adhesion, the velocity obtained in simulations of the lattice model slightly decreases as a function of the adhesion parameter q .

III. THE STRUCTURE OF FRONT INTERFACE

For a sufficiently wide system, patterns can develop along the front interface, perpendicular to the direction of front propagation. This usually occurs when the plane propagating

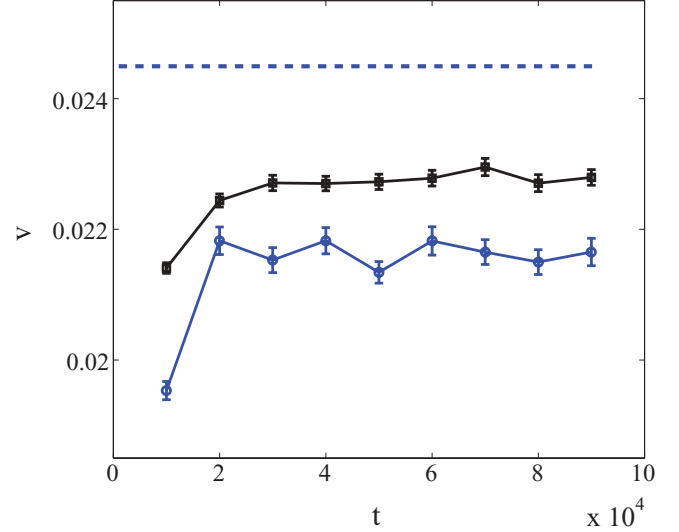


FIG. 3. (Color online) Velocity of front propagation as a function of time as obtained in simulations of the discrete lattice model for $q = 0.1$ (squares) and $q = 0.6$ (circles). The theoretical front speed v_{FK} is shown by the dashed line. $\bar{\alpha} \simeq 0.0006$.

front is unstable to the lateral perturbations, which leads to fingering [18]. Such fingering patterns were also investigated in the context of cell migration and tumor growth [19]. Here we examine the effect of adhesion on a possible formation of fingerlike structures in the lateral direction. It is reasonable to assume that cell-cell adhesion prevents fingering. Indeed, from the macroscopic point of view, it acts as a surface tension [20] and prefers shorter interfaces. From the microscopic point of view, a cell on a tip of a finger has a smaller number of neighbors and therefore easily detaches; this leads again to the planar interfaces.

However, this description is not complete. Consider for a moment the initially uniform system of cells on a two-dimensional lattice (cells on a substrate). It has been recently shown [9] that the system remains uniform only if the cell adhesion parameter q is below a certain threshold q_c , given by

$$u = \frac{1}{2} \pm \frac{1}{2} \left[1 - \frac{16(1 - q_c)^2}{q_c^4} \right]^{1/8}, \quad (6)$$

where u is the (average) cell density. For $q > q_c$, the uniform state becomes unstable [21], and phase separation and clustering occur, resembling phase transition in the Ising model [22]. How does this phenomenon affect front propagation?

The upper panel of Fig. 4 shows the results of simulations of a discrete lattice model for a relatively large (but subcritical, $q < q_c$) value of adhesion parameter. The front interface is rough [23], but no patterns in the lateral (vertical) direction are observed. However, the situation for supercritical adhesion, $q > q_c$, is qualitatively different. Here, cells detaching from the interface and migrating to the invasive region form clusters ahead of the main front. Then the main front propagates and merges with these clusters, but new clusters far from the front are constantly formed; see the lower panel of Fig. 4. The clusters have typical sizes in the lateral direction; the size depends on the interplay between the characteristic time for

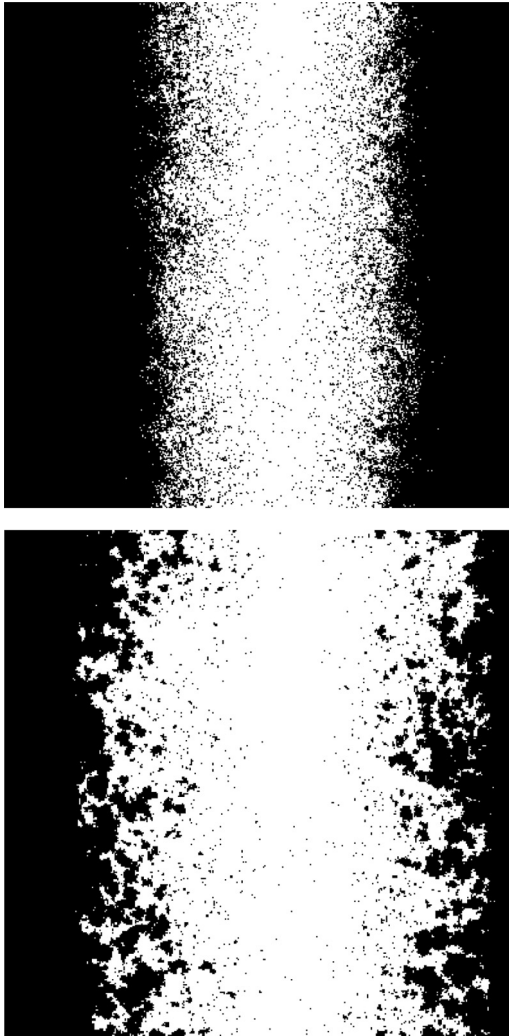


FIG. 4. Front interface for different values of adhesion parameter: $q = 0.6$ (upper panel) and $q = 0.9$ (lower panel). Shown are the simulations of a discrete stochastic lattice model; every black dot represents a cell, and every white dot corresponds to an empty site. The system size is 400×400 (in units of cell diameter), and the proliferation parameter is $\bar{\alpha} = 0.0014$.

cluster formation and growth and the characteristic time for the propagation of the main front. We performed agent-based simulation of the lattice model for various adhesion parameters; the lateral system size (perpendicular to front propagation) was increased up to $H = 3000$ in units of lattice site a . To estimate the typical cluster size, we computed the two-point correlation function $C(x, y) = (1/H) \sum_i [n(x, i)n(x, i + y)]$, where $n(x, y)$ is the occupancy of site (x, y) , and the index i runs from 0 to H . The correlation function was computed at the front interface, at such values of $x = \bar{x}$ where the cell density $u(\bar{x}) = C(\bar{x}, y = 0) = 0.5$. Figure 5 shows the results for various adhesion parameters; one can estimate the lateral cluster size from the characteristic decay length of $C(y) \equiv C(\bar{x}, y)$. The typical decay length for $q < q_c$ is a few lattice sites; for $q > q_c$ macroscopic clusters form. We would like to emphasize that although patterns for $q > q_c$ may resemble fingering, the mechanism for pattern formation is completely different.

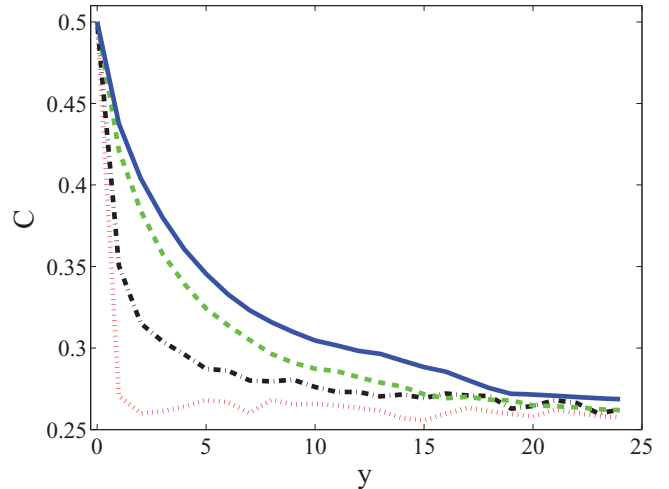


FIG. 5. (Color online) Lateral two-point correlation functions for various adhesion parameters: $q = 0.1$ (dotted line), $q = 0.6$ (dash-dotted line), $q = 0.85$ (dashed line), and $q = 0.9$ (solid line). The proliferation parameter is $\bar{\alpha} = 0.0026$; the simulation time is $t = 3000 \times t_{\text{diff}}$.

The upper panel of Fig. 4 resembles the experimental snapshot shown in Fig. 7 (see below). This is consistent with the subcritical value of the adhesion parameter in these experiments ($q < q_c$). In order to observe clustering in the invasive region (as shown in the lower panel of Fig. 4), one needs to increase cell-cell adhesion above a certain threshold. Although we do not have quantitative experimental data, the experiments with glioma cells transfected to both overexpress and underexpress *N*-cadherins are planned in the near future. This will allow us to compare cell front propagation for small (subcritical) and large (supercritical) values of the adhesion parameter.

The phenomenon of front propagation in a cell population described above can be related to the highly important process of wound healing. In *in vitro* experiments [24], the healing characteristics of scratch wounds made to urothelial cell cultures were investigated in low and in physiological calcium environments. The strength of cell-cell adhesion in experiments was controlled by the concentration of $[\text{Ca}^{2+}]$: lower concentrations of calcium suppressed adhesion, while higher concentrations promoted it. It was observed that cells in the low- $[\text{Ca}^{2+}]$ environment freely and individually migrated into the wounded area, whereas in the case of the high (physiological) calcium concentration, the wound edge moved as a contiguous sheet [24] (see also [25]). It is not clear whether the latter case can be described by our model, since we consider only individual cell migration; in any case, this situation corresponds to $q \simeq 1$. Judging by the structure of the wound edge [24], the case of a low concentration of $[\text{Ca}^{2+}]$ (weaker cell-cell adhesion) seems to correspond to $q < q_c$.

IV. COMPARISON WITH EXPERIMENTS

We have recently performed experiments to investigate the migration of glioma cells on a substrate [6]. Cells were placed on a plastic substrate and a 2 mm scratch was made. Then cells migrated and proliferated into the

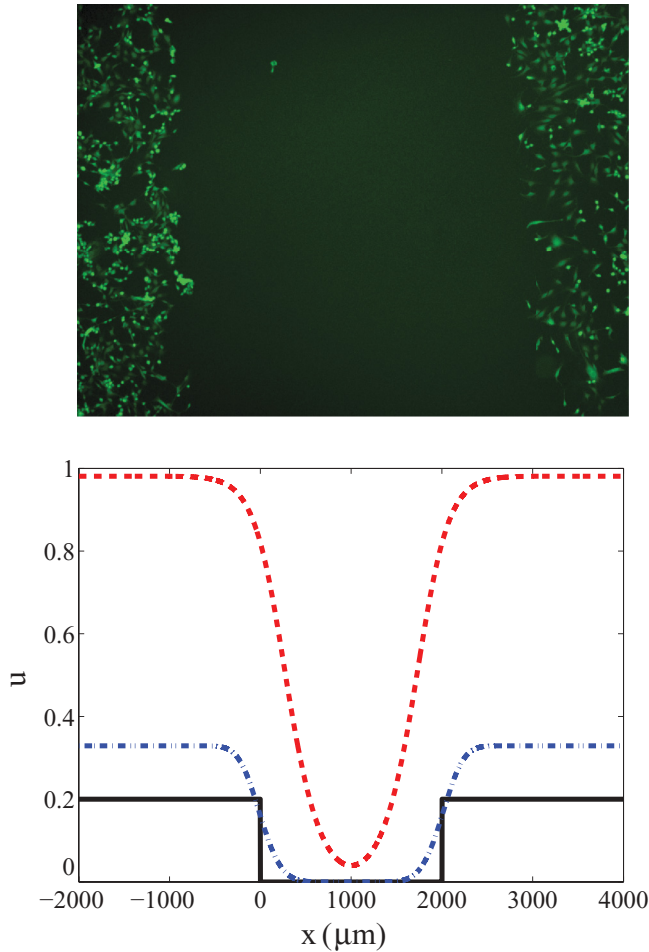


FIG. 6. (Color online) Migration of glioma cells on a substrate. Upper panel: Experimental snapshot at time zero, a view from above. A 2 mm scratch was done at the beginning of experiment. Lower panel: Cell density profiles at different time points after the beginning of the experiment: $t = 0$ (solid line), $t = 24$ h (dash-dotted line), and $t = 120$ h (dashed line). The curves are computed by solving Eq. (4) numerically (in MATLAB) with $\tau = 7.5$ minutes and $\bar{\alpha} = 0.0024 \times (1 + u)^\beta$, $\beta = 1.73$ [6].

gap, and the experiments lasted for 24 hours. To clarify the geometry of the experiment, we present the snapshot of the system (view from above) at the beginning of the experiment; see the upper panel of Fig. 6. Every green dot here is a cell [cells were stained with CellTracker Green (Molecular Probes, OR) to simplify the visualization]. Using experimental observations and simulations of the lattice model, we estimated the parameters for cells both under normoxic and hypoxic conditions [6]. For example, for hypoxic cells, the diffusion time was $\tau \simeq 7.5$ min, the proliferation time was $t_{\text{prolif}} \simeq 53$ h, and the estimated adhesion parameter was $q = 0.1$.

Using these parameters, we numerically computed the density profiles at different times, solving Eq. (4); see the lower panel of Fig. 6. Since the length of experiment (24 h) is comparable to the typical proliferation time (53 h), one cannot expect to observe the established profile of front propagation. Indeed, the profile after 24 h (dash-dotted

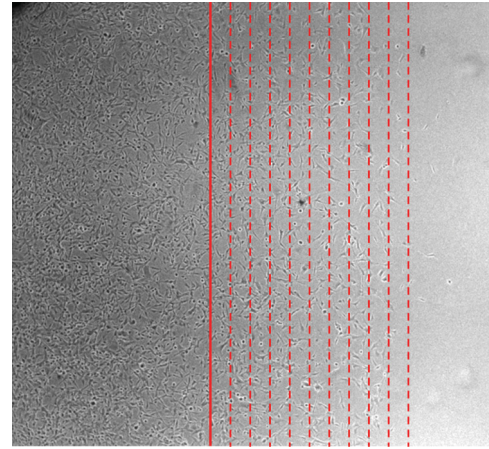


FIG. 7. (Color online) Migration of glioma cells on a substrate, view from above; 72 h from the beginning of the experiment. The approximate initial position of the front edge is shown by the solid line. The system is divided into bins (dashed lines), and the width of every bin is about $110 \mu\text{m}$.

line) is in a transient regime; for comparison, the dashed line (lower panel) shows the density profile after 5 days. A similar transient was observed in a three-dimensional system, where a tumor spheroid was grown in collagen [26].

To make a quantitative comparison between theoretical and experimental results, we performed a new experiment in the same geometry: Migration was measured using a modified scratch-wound healing assay; *U87-MG* cells [27] were plated in 24-well plates at confluence and incubated overnight. Using a 1 mL pipette tip, a scratch was made bisecting the culture well, and one half of the cell monolayer was removed. Remaining cells were imaged at 4x objective after the scratch was made, and each 24 h thereafter for 72 h of incubation. We were able to observe cell migration for 72 h, analyze experimental images, and measure two quantities that characterize the overall distance cells migrated, r_{max} and r_{cm} . To measure r_{max} and r_{cm} , we divided the image into many bins; see Fig. 7. Here, r_{max} is the distance to the most distant bin, averaged over three sets of experiments, while r_{cm} is the distance to the center of mass of the migrating cells: $r_{\text{cm}} = (1/N) \sum_i (n_i r_i)$, where n_i is the number of cells in bin i . Again, the results were averaged over three sets of experiments. We have also performed simulations of the stochastic lattice model, using the phenotypic parameters for *U87-MG* glioma cells obtained in [6]. Employing the same procedure, we measured r_{max} and r_{cm} in simulations; the upper panel of Fig. 8 shows r_{max} and r_{cm} at three time points: 24, 48, and 72 h. We have also computed r_{max} and r_{cm} theoretically, by numerically solving Eq. (4) with a modified proliferation term (see the Appendix).

One can see that there is an excellent agreement between the theoretical results, simulations of the stochastic model, and experimental observations for $r_{\text{max}}(t)$. However, both the theoretical approach and the stochastic model systematically underestimate $r_{\text{cm}}(t)$. The same conclusion follows from the analysis of cell density profiles. The lower panel of Fig. 8 shows the number of cells in a bin as a function of distance 72 h after the beginning of the experiment. One can see that

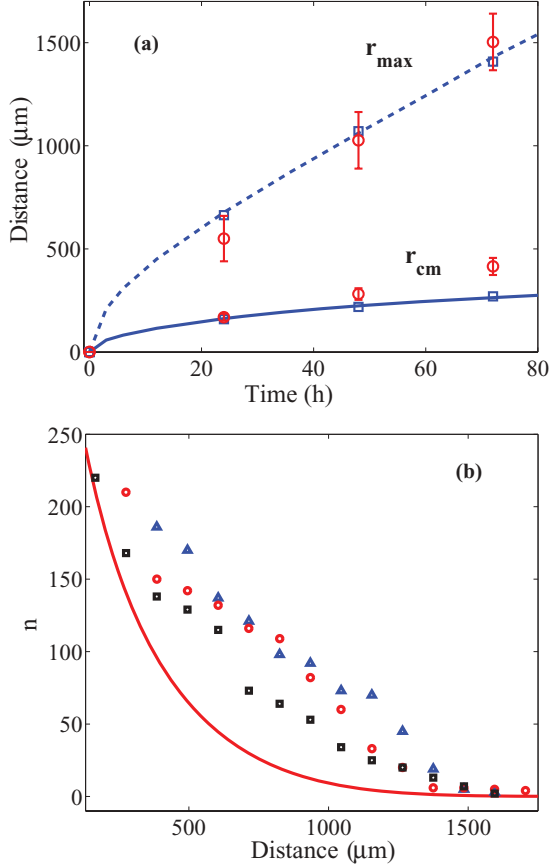


FIG. 8. (Color online) Cell migration: theory and experiments. (a) The distances r_{\max} (upper branch) and r_{cm} (lower branch) vs time from experiments (circles), simulations of stochastic lattice model (squares), and solution of Eq. (4) with a modified proliferation term; see the Appendix (the dashed line corresponds to r_{\max} ; the solid line corresponds to r_{cm}). (b) Number of invasive cells as a function of distance 72 h after the beginning of the experiment. The solid line shows the solution of Eq. (4); the symbols show the results of three sets of experiments. The parameters are $\bar{\alpha} = 0.002$ ($\alpha_0 = 1/29$ 1/h; $t_{\text{diff}} = 3.5$ min), $q = 0.6$.

while the maximal migration distance agrees with the theory, the main mass of cells actually moved much more compared to the predictions of the theory. Therefore, it is likely that there is another important process that affects cell migration and is not taken into account by our modeling. One possible candidate is the phenomenon of chemotaxis: the gradient of chemicals can be small at the tail of the cell density profile (so, the migration of the most advanced cells is only weakly affected), but it can be substantial at the front region, pushing forward the main mass of cells. Investigating this effect is a promising avenue of future research.

V. SUMMARY AND DISCUSSION

In this study, we analyzed the role of cell-cell adhesion in front propagation and the structure of the invasive zone using both the continuum approach and discrete lattice stochastic modeling. We showed that for low adhesion, the asymptotic value of the front velocity, computed from the model with

nonlinear diffusion, is exactly the same as in the FKPP model. Notice, however, that simulations of the discrete lattice model show a slight decrease in the front velocity as cell-cell adhesion is increased. This discrepancy occurs since the correlations were neglected when deriving the nonlinear FKPP equation from the lattice model. Taking into account these correlations is a promising direction of future research.

When the width of a system is large enough, an interesting dynamics can occur in a lateral direction. For supercritical adhesion, the resulting patterns resemble fingering [19], but the mechanisms of pattern formation are completely different. The observed pattern is not related to linear instability of a plane front, but to formation of immobile clusters ahead of the front and subsequent coalescence between the front and the clusters. We plan to investigate this phenomenon in detail using the modified Cahn-Hilliard equation [13]. In order to observe clustering in the invasive region in experiments, one needs to increase cell-cell adhesion above a certain threshold. One way of doing this is transfecting cells to overexpress *N-cadherins*; these experiments are planned for the near future.

We also experimentally investigated the propagation of fronts of glioma cells on a substrate. Both the theoretical results and the results of discrete lattice model simulations successfully reproduced the maximal distance of migration. However, the migration of the main mass of cells was systematically underestimated. This may be an indication of the presence of chemotaxis in the system; we plan to investigate this effect in the future.

ACKNOWLEDGMENTS

E.K. thanks B. Meerson, K. Elder, S. Fedotov, and M. Khasin for fruitful discussions. The research of M.K. was supported by NIH/NCI Grant No. RO1-CA129446. E.K. is grateful to Oakland University for financial support from the URC Faculty Research Fellowship.

APPENDIX : PROLIFERATION

The simplest form of the proliferation term is the usual logistic growth: $\alpha_0 u (1 - u)$. This assumes that the proliferation rate $\alpha_0 (1 - u)$ is a decreasing function of local density u . However, the proliferation rate was found to be more or less constant at small and intermediate densities [6]; it decreases at high densities due to the contact inhibition effect [28]. There are many ways to model this behavior by introducing an additional parameter; for example, the generalized (Richards) logistic growth $\alpha_0 u (1 - u^v)$ was employed in [29]. It is, however, not clear how this term can be derived from the stochastic lattice model. It is convenient to have a discrete microscopic analog of the proliferation term; here we construct such an analog. Assuming a two-dimensional square lattice, we consider the most general case: let α_0 be the probability of proliferation in case a cell does not have neighbors, α_1 be the probability of proliferation in case a cell has one neighbor, α_2 be the probability of proliferation in case a cell

has two neighbors, and α_3 be the probability of proliferation in case a cell has three neighbors. This leads to the following macroscopic equation:

$$\frac{du}{dt} = u(1-u)[\alpha_0(1-u)^3 + 3\alpha_1u(1-u)^2 + 3\alpha_2u^2(1-u) + \alpha_3u^3].$$

Since it is sufficient to have just one additional parameter to fit the experimental results (besides the basic proliferation rate α_0), one can choose the probabilities of proliferation in the discrete model to be $\alpha_1 = \gamma\alpha_0$, $\alpha_2 = \gamma^2\alpha_0$, and $\alpha_3 = \gamma^3\alpha_0$. $\gamma = 1$ corresponds to the usual logistic growth; certain values of $\gamma > 1$ are consistent with the observation that the proliferation rate is more or less constant at small and intermediate densities and decreases at high densities. In this case, we have

$$\frac{du}{dt} = \alpha_0u(1-u)[(1-u)^3 + 3\gamma u(1-u)^2 + 3\gamma^2u^2(1-u) + \gamma^3u^3]. \quad (\text{A1})$$

In a recent experiment, *U87* glioma cell were placed uniformly on a substrate and their number was measured as a function of time. Figure 9 shows both experimental results [6], the density $u(t)$ computed from Eq. (A1), and the results from simulations of the discrete lattice model for $\gamma = 1.52$. An excellent agreement between the two theoretical approaches

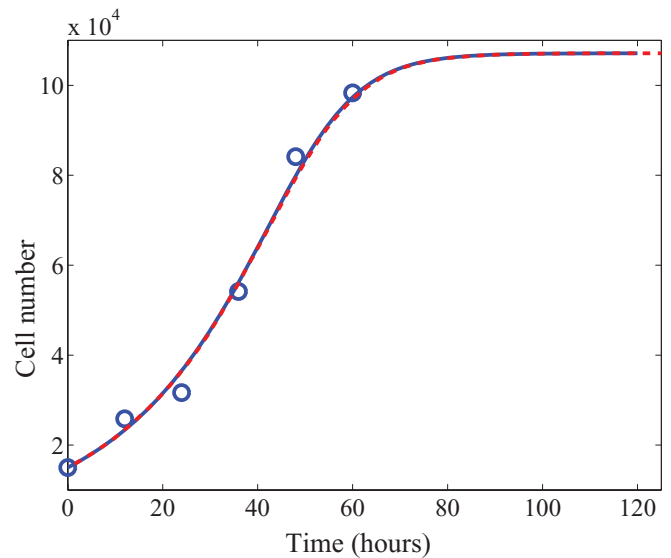


FIG. 9. (Color online) *U87* glioma cell proliferation on a substrate: cell number as a function of time. Circles show experimental results for cell proliferation [6]; solid curve shows a theoretical fit given by Eq. (A1); dashed curve shows the results of discrete lattice modeling. The parameters are $u_0 = 0.14$, $\alpha_0 = 1/29 \text{ h}^{-1}$, $\gamma = 1.52$.

and the experimental results is observed. The same values of α_0 and γ were used in Fig. 8.

- [1] E. C. Holland, *Proc. Natl. Acad. Sci. USA* **97**, 6242 (2000).
- [2] CBTRUS (2002). Statistical Report: Primary Brain Tumors in the United States, 1995–1999. Published by the Central Brain Tumor Registry of the United States, <http://www.cbtrus.org/reports/2002/2002report.pdf>.
- [3] A. Giese, R. Bjerkvig, M. E. Berens, and M. Westphal, *J. Clin. Oncol.* **21**, 1624 (2003).
- [4] R. A. Fisher, *Annu. Eugenics* **7**, 355 (1937); A. Kolmogorov, I. Petrovsky, and N. Piscounov, *Moscow Univ. Bull. Math.* **1**, 1 (1937).
- [5] M. Bramson, P. Calderoni, A. Demasi, P. Ferrari, J. Lebowitz, and R. H. Schonmann, *J. Stat. Phys.* **45**, 905 (1986).
- [6] E. Khain, M. Katakowski, S. Hopkins, A. Szalad, X. G. Zheng, F. Jiang, and M. Chopp, *Phys. Rev. E* **83**, 031920 (2011).
- [7] J. D. Murray, *Mathematical Biology. II: Spatial Models and Biomedical Applications*, 3rd ed. (Springer, New York Berlin Heidelberg, 2003).
- [8] K. R. Swanson, E. C. Alvord, and J. D. Murray, *Cell Prolif.* **33**, 317 (2000); K. R. Swanson, C. Bridge, J. D. Murray, and E. C. Alvord, *J. Neurol. Sci.* **216**, 1 (2003); K. R. Swanson, R. C. Rostomily, and E. C. Alvord, *Br. J. Cancer* **98**, 113 (2008).
- [9] E. Khain, C. M. Schneider-Mizell, M. O. Nowicki, E. A. Chiocca, S. E. Lawler, and L. M. Sander, *Europhys. Lett.* **88**, 28006 (2009).
- [10] X. Zheng, F. Jiang, M. Katakowski, X. P. Zhang, H. Jiang, Z. G. Zhang, and M. Chopp, *Cancer Lett.* **265**, 177 (2008).
- [11] S. Turner, J. A. Sherratt, K. J. Painter, and N. J. Savill, *Phys. Rev. E* **69**, 021910 (2004); S. Turner, *ibid.* **71**, 041903 (2005); M. Alber, N. Chen, T. Glimm, and P. M. Lushnikov, *ibid.* **73**, 051901 (2006); N. J. Armstrong, K. J. Painter, and J. A. Sherratt, *J. Theor. Biol.* **243**, 98 (2006); C. Deroulers, M. Aubert, M. Badoual, and B. Grammaticos, *Phys. Rev. E* **79**, 031917 (2009).
- [12] E. Khain, L. M. Sander, and C. M. Schneider-Mizell, *J. Stat. Phys.* **128**, 209 (2007).
- [13] E. Khain and L. M. Sander, *Phys. Rev. E* **77**, 051129 (2008).
- [14] M. J. Simpson, C. Towne, D. L. Sean McElwain, and Z. Upton, *Phys. Rev. E* **82**, 041901 (2010).
- [15] S. Fedotov, *Phys. Rev. E* **58**, 5143 (1998); **59**, 5040 (1999).
- [16] U. Ebert and W. van Saarloos, *Phys. D* **146**, 1 (2000); W. van Saarloos, *Phys. Rep.* **386**, 29 (2003).
- [17] T. Callaghan, E. Khain, L. M. Sander, and R. M. Ziff, *J. Stat. Phys.* **122**, 909 (2006).
- [18] A. P. Aldushin and B. J. Matkowsky, *Combust. Sci. Technol.* **133**, 293 (1998); W. van Saarloos, *Phys. Rep.* **386**, 29 (2003); T. Bansagi, D. Horvath, and A. Toth, *J. Chem. Phys.* **121**, 11912 (2004).
- [19] E. Khain and L. M. Sander, *Phys. Rev. Lett.* **96**, 188103 (2006); G. Y. Ouaknin and P. Z. Bar-Yoseph, *Biophys. J.* **97**, 1811 (2009); N. Poplawski, U. Agero, J. Gens, M. Swat, J. A. Glazier, and A. R. Anderson, *Bull. Math. Biol.* **71**, 1189 (2009); J. Lowengrub, H. Frieboes, F. Jin, Y. Chuang, X. Li, P. Macklin, S. Wise, and V. Cristini, *Nonlinearity* **23**, R1 (2010); P. Gerlee and A. R. A. Anderson, *Math. Biosci. Eng.* **7**, 385 (2010).

- [20] R. A. Foty and M. S. Steinberg, *Dev. Biol.* **278**, 255 (2005); B. Hegedus, F. Marga, K. Jakab, K. L. Sharpe-Timms, and G. Forgacs, *Biophys. J.* **91**, 2708 (2006).
- [21] J. S. Langer, in *Solids Far from Equilibrium*, edited by C. Godreche (Cambridge University Press, New York, 1992), pp. 297–364.
- [22] K. Huang, *Statistical Mechanics* (Wiley, New York, 1987).
- [23] M. Block, E. Scholl, and D. Drasdo, *Phys. Rev. Lett.* **99**, 248101 (2007).
- [24] D. C. Walker, G. Hill, S. M. Wood, R. H. Smallwood, and J. Southgate, *IEEE Trans. Nanobiosci.* **3**, 153 (2004).
- [25] S. Mark, R. Shlomovitz, N. S. Gov, M. Poujade, E. Grasland-Mongrain, and P. Silberzan, *Biophys. J.* **98**, 361 (2010).
- [26] E. Khain, L. M. Sander, and A. Stein, *Complexity* **11**, 53 (2005).
- [27] *U87-MG* cells were obtained from the American Type Culture Collection (Manassas, VA). Cells were maintained in Dulbecco's Modified Eagle Medium supplemented with 10% fetal bovine serum.
- [28] A. Puliafito, L. Hufnagel, P. Neveu, S. Streichan, A. Sigal, D. K. Fygenson, and B. I. Shraiman, *Proc. Natl. Acad. Sci. USA* **109**, 739 (2012).
- [29] M. J. Simpson, A. Merrifield, K. A. Landman, and B. D. Hughes, *Phys. Rev. E* **76**, 021918 (2007).